

# Swin fMRI Transformer Predicts Early Neurodevelopmental Outcomes from Neonatal fMRI

Patrick Styll<sup>\*1</sup>, Dowon Kim<sup>\*2</sup> and Jiook Cha<sup>2</sup>

<sup>1</sup>Technical University of Vienna  
patrick.styll@tuwien.ac.at

<sup>2</sup>Seoul National University  
{dowonkim00, connectome}@snu.ac.kr

## Abstract

Brain development in the first few months of human life is a critical phase characterized by rapid structural growth and functional organization. Accurately predicting developmental outcomes during this time is crucial for identifying delays and enabling timely interventions. This study introduces the SwiFT (Swin 4D fMRI Transformer) model, designed to predict Bayley-III composite scores using neonatal fMRI data from the Developing Human Connectome Project (dHCP). To enhance predictive accuracy, we apply dimensionality reduction via group independent component analysis (ICA) and pretrain SwiFT on large adult fMRI datasets to address the challenges of limited neonatal data. Our analysis shows that SwiFT significantly outperforms baseline models in predicting cognitive, motor, and language outcomes, leveraging both single-label and multi-label prediction strategies. The model's attention-based architecture processes spatiotemporal data end-to-end, delivering superior predictive performance. Additionally, we use Integrated Gradients with Smoothgrad sQuare (IG-SQ) to interpret predictions, identifying neural spatial representations linked to early cognitive and behavioral development. These findings underscore the potential of Transformer models to advance neurodevelopmental research and clinical practice.

## 1 Introduction

Brain development during the first few months of life is a period of rapid structural and functional reorganization, making it a critical window for identifying potential neurodevelopmental deficits. Accurately predicting developmental outcomes during this period is essential for enabling early interventions that can mitigate the lifelong impact of developmental delays. Neonatal fMRI data, such as those from the Developing Human Connectome Project (dHCP), have shown potential for predicting neurodevelopmental outcomes (Li et al. 2024) (Xia et al. 2024) (Gondová et al. 2023) (Eyre et al. 2021). However, the spatiotemporal complexity of neonatal brain activity presents significant challenges for conventional analysis methods.

This study investigates the potential of the Swin 4D fMRI Transformer (SwiFT) (Kim et al. 2023), a deep learning architecture designed to process high-dimensional fMRI data, for predicting neurodevelopmental outcomes from neonatal

fMRI. Specifically, we aim to predict Bayley Scales of Infant and Toddler Development, Third Edition (Bayley-III/BSID-III) composite scores, encompassing cognitive, language, and motor skills, using neonatal fMRI from the dHCP dataset. To address the challenges of limited neonatal data and high dimensionality, we explore dimensionality reduction using group Independent Component Analysis (ICA) and pretraining SwiFT on large publicly available adult fMRI datasets.

We hypothesize that (1) SwiFT will outperform existing baseline models in predicting Bayley-III scores due to its ability to capture complex spatiotemporal patterns in fMRI data and (2) incorporating ICA features and pretraining will further improve predictive accuracy. We further aim to interpret SwiFT's predictions using Integrated Gradients with Smoothgrad sQuare (IG-SQ) (Rahman et al. 2022) (Adebayo et al. 2018) (Kokhlikyan et al. 2020) to identify brain regions associated with early cognitive, language, and motor development.

This research advances the state of neurodevelopmental prediction by introducing a robust and interpretable framework for neonatal fMRI analysis. By addressing key methodological challenges, our findings lay the groundwork for future applications in neurodevelopmental research and clinical practice.

In Section 2, we introduce the dataset, its acquisition, (additional) processing and target values. We also explain the SwiFT Transformer, our motivations and how we will interpret the results of the model. In Section 3, we will explain in what settings we perform our experiments, and introduce (i) the baselines, (ii) SwiFT running on (pre-processed) raw fMRI data with single-label and multi-label prediction, and (iii) SwiFT running on group-ICA-extracted features with single-label and multi-label prediction. In the end, we give an overview of the performance gain through our methods. In Section 4, we perform IG-SQ on the best performing model and provide our interpretation of the IG maps on risk of delay in cognitive, language and motor skills. Moreover, we provide a small glimpse into what model interpretations on brain-network-level may look like by using ICA-extracted features. Lastly, we conclude our research in Section 5 through discussing future directions and limitations of our current work.

<sup>\*</sup>These authors contributed equally.

## 2 Methods

**Target Developmental Outcomes** This study focuses on Bayley Scales of Infant and Toddler Development, Third Edition (Bayley-III), composite scores in cognitive, language, and motor domains. Developmental delays are categorized based on established thresholds (Johnson, Moore, and Marlow 2014):

- greater than or equal to 85: average development
- lower than 85: risk of developmental delay
- lower than 75: moderate to severe mental impairment

Following prior studies (He et al. 2018) (He et al. 2020a), we simplify the classification task into a binary format, with a threshold of 85 distinguishing low- and high-risk cases. Regression tasks are also conducted to predict continuous Bayley-III scores, providing finer-grained insights into developmental outcomes. By integrating these approaches, we aim to enhance the accuracy and interpretability of predictions using SwiFT.

**Dataset** The Developing Human Connectome Project (dHCP) dataset provides a rich and representative basis for developing predictive models of early neurodevelopment. It includes 783 neonates born between 23–44 gestational weeks, with imaging performed between 26–45 post-menstrual weeks. Resting-state fMRI (rs-fMRI) data were acquired using a 3T Philips Achieva scanner and pre-processed via the dHCP pipeline for motion correction, denoising, and spatial normalization.

For this study, Bayley-III scores in cognition, motor, and language domains were available for 739 infants, with 619 of them also having usable fMRI data. The composite scores showed a mean close to 100, with imbalances in developmental delay cases:  $\approx 5\%$  for motor and cognitive domains and  $\approx 18\%$  for language. Strong positive correlations were observed between cognitive, motor, and language scores (63.08%, 57.27%, and 51.94%, respectively). Maternal factors (e.g., smoking) showed no significant correlation with scores.

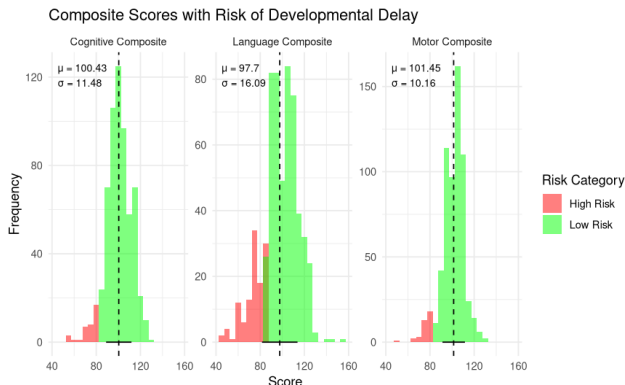


Figure 1: Distributions of composite scores based on binary classification. Assumptions made in (Johnson, Moore, and Marlow 2014) largely hold true.

**MRI Acquisition and Processing** MRI data were acquired on a 3T Philips Achieva system with a neonatal 32-channel head coil. The imaging protocol was tailored to the unique characteristics of the neonatal brain, which has different tissue properties compared to the adult brain, including higher water content and longer T1 and T2 relaxation times. Resting-state fMRI (rs-fMRI) was captured with a multiband-accelerated echo-planar imaging sequence (TR: 392 ms, TE: 38 ms, resolution: 2.15 mm<sup>3</sup>) over roughly 15 minutes (2300 volumes). Processing followed the dHCP pipeline, which is specifically designed to address the challenges of neonatal imaging. This included motion and distortion correction, skull stripping, ICA-based denoising with FIX, and high-pass temporal filtering to remove slow drifts.

To align the data to a neonatal-specific template space, we adopted a pipeline inspired by the automated resting-state functional framework developed for the dHCP dataset (Fitzgibbon et al. 2020). Specifically, we utilized the 40-week T1-weighted template from the extended dHCP Augmented Volumetric Atlas (Schuh et al. 2018), down-sampled from a spatial resolution of 0.5 mm<sup>3</sup> isotropic to 2.15 mm<sup>3</sup> isotropic to match the native resolution of the fMRI images. Image registration was performed using ANTs (Tustison et al. 2021) on the mean image of all time-points, with the resulting transformation applied independently to each timeframe in parallel (Tange 2023). The processed outputs served as inputs for the subsequent experiments.

**Swin fMRI Transformer** To predict neurodevelopmental outcomes from neonatal fMRI, we employed SwiFT, a Transformer-based architecture designed to model high-dimensional spatiotemporal fMRI data. SwiFT processes raw 4D fMRI volumes, capturing local and global dependencies critical for neurodevelopmental predictions. The model operates by dividing 4D fMRI data into patches, embedding them as tokens, and processing these tokens through multiple layers of 4D Swin Transformer blocks. These blocks utilize a shifted window multi-head self-attention mechanism, enabling efficient modeling of complex spatiotemporal patterns while reducing computational complexity through patch merging. Previously, SwiFT demonstrated robust performance on diverse fMRI tasks, including sex classification (97.7% accuracy on HCP) and age prediction (MAE of 3.40 years on UK Biobank), showcasing its effectiveness in capturing brain dynamics across populations.

## 3 Experiments

### 3.1 Experimental Settings

All experiments were conducted on the *Perlmutter* supercomputer, an HPE Cray EX system. A holdout strategy with a 70:15:15 data split was used for training, validation, and testing. To address dataset imbalance (see Section 2), stratified splits were applied based on BSID-III scores. For benchmarking, stratified 5-fold cross-validation ensured consistent and fair splits across experiments.

For binary classification, we used weighted focal loss (Lin et al. 2018) to prioritize harder-to-classify (*at-risk*) cases.

This approach significantly improved performance, especially for these challenging instances.

Following the original SwiFT paper (Kim et al. 2023), we padded input images to 64x64x64 to align with the model architecture, adapting from the 96x96x96 padding used in the original work due to our native image size of 45x55x45.

For classification tasks, we evaluated performance using the area under the ROC curve (AUC), accuracy, and balanced accuracy ( $ACC_{bal}$ ) to account for class imbalance. For regression tasks, mean absolute error (MAE) and mean squared error (MSE) were used, along with adjusted metrics ( $MAE_{adj}$  and  $MSE_{adj}$ ) to reflect re-scaled values for interpretability.

### 3.2 Baselines

We established baseline performance using ROI-based deep learning models, including BrainNetCNN (Kawahara et al. 2017), VanillaTF, and Brain Network Transformer (BNT) (Kan et al. 2022), which take functional connectivity matrices as input (computed via Pearson correlations of 87 brain regions in the dHCP neonatal brain atlas). Hyper-parameters and implementations followed (Kan et al. 2022). Additionally, we included XGBoost (Chen and Guestrin 2016) as a traditional machine learning baseline, using the flattened upper triangular correlation matrix as input.

Table 1: Mean regression performance of each baseline model with standard deviation through 5-fold cross-validation

Model	Cog		
	$MSE_{adj}$	MAE	$MAE_{adj}$
XGBoost	155.6 $\pm$ 15.0	<b>0.84<math>\pm</math>0.03</b>	<b>9.59<math>\pm</math>0.48</b>
BrainNetCNN	<b>113.6<math>\pm</math>54.2</b>	0.84 $\pm$ 0.09	9.66 $\pm$ 1.55
VanillaTF	210.1 $\pm$ 91.4	0.91 $\pm$ 0.04	10.43 $\pm$ 1.13
BNT	147.1 $\pm$ 86.7	0.87 $\pm$ 0.07	10.01 $\pm$ 1.33

Model	Lang		
	$MSE_{adj}$	MAE	$MAE_{adj}$
XGBoost	304.7 $\pm$ 33.9	<b>0.86<math>\pm</math>0.07</b>	<b>13.94<math>\pm</math>0.75</b>
BrainNetCNN	317.6 $\pm$ 109.6	0.88 $\pm$ 0.04	14.28 $\pm$ 1.31
VanillaTF	<b>279.7<math>\pm</math>96.3</b>	0.91 $\pm$ 0.03	14.77 $\pm$ 1.21
BNT	355.1 $\pm$ 49.6	0.90 $\pm$ 0.03	14.68 $\pm$ 1.20

Model	Mot		
	$MSE_{adj}$	MAE	$MAE_{adj}$
XGBoost	124.9 $\pm$ 18.0	<b>0.81<math>\pm</math>0.05</b>	<b>8.55<math>\pm</math>0.59</b>
BrainNetCNN	<b>115.74<math>\pm</math>28.5</b>	0.84 $\pm$ 0.04	8.93 $\pm$ 0.75
VanillaTF	173.0 $\pm$ 108.2	0.86 $\pm$ 0.03	9.11 $\pm$ 0.84
BNT	153.7 $\pm$ 100.4	0.81 $\pm$ 0.04	8.58 $\pm$ 0.90

### 3.3 fMRI Volumes

We evaluated the SwiFT model’s performance on fMRI data in an end-to-end manner, focusing on single-label and multi-label prediction tasks. Multi-label prediction was hypothesized to enhance performance due to strong correlations among Bayley scores (see Section 2), as supported by prior work (He et al. 2020b).

The models were fine-tuned across a predefined hyperparameter search space, including data augmentation strategies (affine-only, intensity-only, and combined transformations),

Table 2: Mean classification performance of each baseline model with standard deviation through 5-fold cross-validation.

Model	Cog		
	$ACC_{bal}$	ACC	AUC
XGBoost	50.0 $\pm$ 0.0	<b>93.8<math>\pm</math>0.4</b>	51.5 $\pm$ 10.4
BrainNetCNN	49.6 $\pm$ 0.4	93.0 $\pm$ 1.0	47.5 $\pm$ 4.8
VanillaTF	<b>52.2<math>\pm</math>4.2</b>	92.5 $\pm$ 1.0	55.5 $\pm$ 9.5
BNT	51.2 $\pm$ 3.7	93.1 $\pm$ 1.0	<b>59.8<math>\pm</math>4.2</b>

Model	Lang		
	$ACC_{bal}$	ACC	AUC
XGBoost	50.0 $\pm$ 0.9	<b>79.5<math>\pm</math>0.8</b>	50.4 $\pm$ 7.5
BrainNetCNN	50.3 $\pm$ 3.0	77.5 $\pm$ 3.1	<b>56.1<math>\pm</math>4.9</b>
VanillaTF	49.9 $\pm$ 2.4	74.0 $\pm$ 2.4	54.1 $\pm$ 6.8
BNT	<b>51.1<math>\pm</math>3.9</b>	74.8 $\pm$ 3.1	<b>57.1<math>\pm</math>5.6</b>

Model	Mot		
	$ACC_{bal}$	ACC	AUC
XGBoost	<b>49.7<math>\pm</math>0.3</b>	<b>93.1<math>\pm</math>0.5</b>	51.2 $\pm$ 6.2
BrainNetCNN	49.5 $\pm$ 0.7	92.7 $\pm$ 1.3	<b>57.1<math>\pm</math>5.6</b>
VanillaTF	49.2 $\pm$ 0.4	92.1 $\pm$ 0.8	47.4 $\pm$ 7.9
BNT	49.5 $\pm$ 0.3	92.7 $\pm$ 0.7	44.7 $\pm$ 6.8

learning rates, batch sizes, and patch sizes. Sequence length was varied to evaluate its impact: a baseline length of 20 was used per the original SwiFT paper (Kim et al. 2023), with additional experiments using lengths of 50 and 100 to assess temporal dynamics. Longer sequences have shown promise in prior studies for predicting intelligence in young adults and elders (Kim et al. 2023).

To leverage publicly available fMRI datasets, we pre-trained SwiFT using contrastive self-supervised learning (Dave et al. 2022) on data from the UK Biobank (UKB)(Alfaro-Almagro et al. 2018b; Miller et al. 2016a), Human Connectome Project (HCP)(Van Essen et al. 2013), and Adolescent Brain Cognitive Development (ABCD) study(Casey et al. 2018). While this approach utilizes larger datasets, differences between neonatal and adult or adolescent brain data present potential limitations. To address size discrepancies, neonatal images were padded to 96x96x96, contrasting with experiments trained from scratch, where images were padded to 64x64x64 (see Section 3.1).

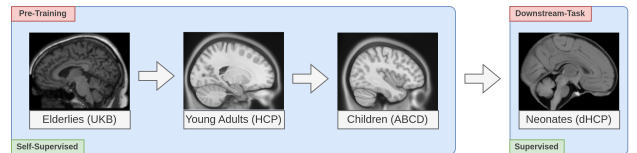


Figure 2: Rationale of using large amounts of brain fMRI data across different datasets to make up for the little amount of data available for neonates.

**Single-Label Prediction** The choice of sequence length had a notable impact on the model’s performance. A length of 50 yielded the best results, while shorter (20) or longer

(100) sequences performed slightly worse, suggesting that an optimal balance is necessary.

As shown in Table 3, pre-training resulted in only minor improvements in predictive power for BSID-III scores. However, increased padding might have negatively influenced performance. Compared to baseline models, SwiFT provided significant performance gains for both regression and classification tasks. For cognitive and language predictions, adjusted MAE improved by approximately 11%, while gains for motor regression were minimal. In classification, balanced accuracy ( $ACC_{bal}$ ) improved by 5-7% points, exceeding guessing levels.

Table 3: Mean performance with standard deviation through 5-cross-validation by using raw fMRI, facilitating single-label predictions.

Method	Cog		
	$MSE_{adj}$	MAE	$MAE_{adj}$
Scratch	127.8 $\pm$ 11.8	0.77 $\pm$ 0.03	8.8 $\pm$ 0.7
Pre-Tr.	<b>123.5<math>\pm</math>12.6</b>	<b>0.76<math>\pm</math>0.02</b>	<b>8.6<math>\pm</math>0.5</b>
	ACC	$ACC_{bal}$	AUC
Scratch	94.4 $\pm$ 0.7	<b>54.9<math>\pm</math>3.8</b>	<b>56.9<math>\pm</math>5.2</b>
Pre-Tr.	<b>94.9<math>\pm</math>1.2</b>	54.1 $\pm$ 3.6	54.6 $\pm$ 3.2
Method	Lang		
	$MSE_{adj}$	MAE	$MAE_{adj}$
Scratch	293.4 $\pm$ 20.1	0.79 $\pm$ 0.04	12.9 $\pm$ 0.5
Pre-Tr.	<b>287.4<math>\pm</math>15.4</b>	<b>0.78<math>\pm</math>0.02</b>	<b>12.6<math>\pm</math>0.3</b>
	ACC	$ACC_{bal}$	AUC
Scratch	82.7 $\pm$ 2.8	56.2 $\pm$ 2.1	<b>56.6<math>\pm</math>3.2</b>
Pre-Tr.	<b>83.9<math>\pm</math>1.4</b>	<b>57.6<math>\pm</math>3.1</b>	56.3 $\pm$ 3.1
Method	Mot		
	$MSE_{adj}$	MAE	$MAE_{adj}$
Scratch	<b>103.1<math>\pm</math>9.2</b>	<b>0.81<math>\pm</math>0.08</b>	<b>8.4<math>\pm</math>0.9</b>
Pre-Tr.	105.7 $\pm$ 9.8	0.82 $\pm$ 0.09	8.6 $\pm$ 1.1
	ACC	$ACC_{bal}$	AUC
Scratch	<b>93.6<math>\pm</math>0.6</b>	54.2 $\pm$ 3.2	55.5 $\pm$ 3.7
Pre-Tr.	92.8 $\pm$ 1.2	<b>55.1<math>\pm</math>3.3</b>	<b>55.7<math>\pm</math>3.9</b>

**Multi-Label Prediction** To predict all three classes simultaneously, we used a shared classification/regression head, a design choice based on the expected correlation among these values (see Section 2).

Sequence length changes showed similar effects to single-label predictions. As shown in Table 4, pre-training provided only marginal improvements, highlighting the limited transferability of adult data to neonatal predictions. However, multi-label regression results align with previous studies (He et al. 2020b), showing performance gains across all classes for both regression and classification. These improvements may stem from shared learning across developmental domains, enabling the model to capture complex, interrelated features of early brain development.

Table 4: Mean performance with standard deviation through 5-cross-validation by using raw fMRI, facilitating multi-label predictions.

Method	Cog		
	$MSE_{adj}$	MAE	$MAE_{adj}$
Scratch	125.7 $\pm$ 16.6	<b>0.64<math>\pm</math>0.07</b>	<b>8.5<math>\pm</math>0.6</b>
Pre-Tr.	<b>119.2<math>\pm</math>12.6</b>	0.64 $\pm$ 0.12	8.6 $\pm$ 1.2
	ACC	$ACC_{bal}$	AUC
Scratch	<b>96.4<math>\pm</math>1.0</b>	59.7 $\pm$ 2.1	62.6 $\pm$ 4.0
Pre-Tr.	95.6 $\pm$ 2.4	<b>66.0<math>\pm</math>2.9</b>	<b>62.7<math>\pm</math>4.7</b>
Method	Lang		
	$MSE_{adj}$	MAE	$MAE_{adj}$
Scratch	212.4 $\pm$ 17.7	0.87 $\pm$ 0.05	11.6 $\pm$ 0.7
Pre-Tr.	<b>205.3<math>\pm</math>15.3</b>	<b>0.86<math>\pm</math>0.07</b>	<b>11.5<math>\pm</math>0.9</b>
	ACC	$ACC_{bal}$	AUC
Scratch	83.3 $\pm$ 1.5	61.7 $\pm$ 1.7	62.0 $\pm$ 1.9
Pre-Tr.	<b>83.7<math>\pm</math>1.3</b>	<b>62.3<math>\pm</math>1.9</b>	<b>63.2<math>\pm</math>2.2</b>
Method	Mot		
	$MSE_{adj}$	MAE	$MAE_{adj}$
Scratch	<b>99.8<math>\pm</math>15.3</b>	<b>0.56<math>\pm</math>0.03</b>	<b>7.4<math>\pm</math>0.5</b>
Pre-Tr.	103.0 $\pm$ 13.2	0.57 $\pm$ 0.04	7.6 $\pm$ 0.6
	ACC	$ACC_{bal}$	AUC
Scratch	95.2 $\pm$ 0.7	<b>57.8<math>\pm</math>2.1</b>	<b>59.7<math>\pm</math>1.7</b>
Pre-Tr.	<b>95.2<math>\pm</math>0.5</b>	56.3 $\pm$ 1.9	58.9 $\pm$ 1.9

### 3.4 Dimensionality Reduction via Group ICA

Group Independent Component Analysis (Group ICA) (Hyvärinen 1999; Beckmann and Smith 2004) is a widely used data-driven technique in neuroimaging that decomposes fMRI data into independent spatial and temporal components. These components represent distinct neural processes or functional networks. Group ICA reduces the dimensionality of high-dimensional fMRI data while preserving significant information and isolating biologically interpretable brain networks.

In this study, we use Group ICA features as model inputs for both single-label and multi-label learning. These features encapsulate complex brain activity patterns in a compact representation, enhancing expressiveness and facilitating brain network-level analysis. We hypothesize that this approach will improve model interpretability and predictive performance by leveraging the reduced dimensionality and biologically relevant features.

#### Preparation

**Data Sampling** To generate the Group ICA map, we selected a subset of normally developing neonates, defined as those with cognitive, language, and motor BSID-III scores above 85, indicating low risk of developmental delay. Only normally developing data were used to reduce variability and noise, ensuring a more reliable feature set.

Out of 725 assessed subjects, 431 met the criteria for normal development, with 358 having usable fMRI data. To further enhance stability, we excluded neonates with gesta-

tional ages outside 36 to 44 weeks, as defined by the dHCP volumetric atlas (Schuh et al. 2018), resulting in a final cohort of 348 subjects. From this group, we randomly selected 100 neonates for Group ICA analysis.

**Group ICA and Dimensionality Reduction** The workflow for Group ICA and functional connectivity analysis (see Figure 3) follows methodologies established for the UKB dataset (Alfaro-Almagro et al. 2018a; Miller et al. 2016b). For the selected 100 subjects, we used MIGP (MELODIC’s Incremental Group-PCA) to extract the top 1200 weighted spatial eigenvectors, approximating traditional PCA while remaining computationally efficient for large datasets (Smith et al. 2014). Spatial Independent Component Analysis (spatial-ICA) was then applied using FSL MELODIC (Hyvärinen 1999; Beckmann and Smith 2004) to parcellate the data into spatially independent components (ICs). We evaluated dimensionalities of 25 and 100 ICs, consistent with prior work on the UKB dataset (Alfaro-Almagro et al. 2018a; Miller et al. 2016b; Smith et al. 2013, 2009). Higher dimensionalities result in smaller, more numerous regions within spatial maps. Since FIX denoising was performed during preprocessing, we did not identify artifactual components, assuming their removal.

Using the generated group ICA maps, we performed dual regression to obtain subject-specific spatial maps for each IC. Dual regression comprises two steps: (i) spatial regression, projecting group-level IC maps onto individual data, and (ii) temporal regression, deriving subject-specific time-series for each IC. To further explore functional connectivity, we conducted seed-to-voxel (seed2voxel) analysis, correlating timeseries of specific brain regions with those of all other voxels. The resulting whole-brain functional connectivity maps served as input features for the SwiFT model to predict neurodevelopmental outcomes.

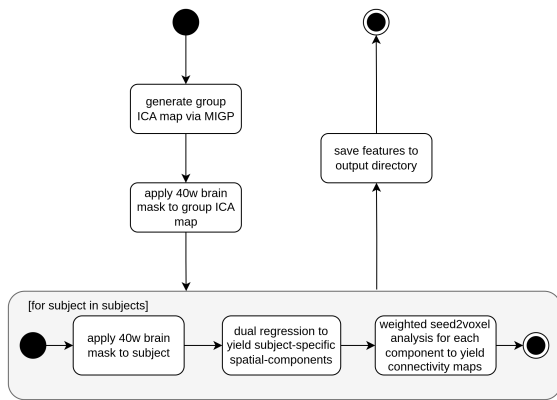


Figure 3: UML Flowchart depicting the workflow to extract features and connectivity maps by leveraging Group Independent Component Analysis, heavily inspired by (Alfaro-Almagro et al. 2018a), (Miller et al. 2016b) and (Gal et al. 2022).

## Results

**Training Process** For each dimensionality, the model was tuned using a predefined hyperparameter search space, including learning rate, patch size, and data augmentation strategies (see Section 3.3). With ICA reducing the input data to a fraction of its original dimensionality, careful tuning was critical to ensure effective convergence. Given the data demands of transformer architectures and the reduced training data size, we increased the maximum training epochs to 100. To mitigate overfitting, we applied data augmentation techniques such as affine and intensity transformations to enhance sample diversity and improve generalizability. Due to the specific sequence lengths required for IC-based training (42 and 100), transfer learning was not utilized in these experiments.

We addressed potential data leakage by ensuring that the 100 healthy subjects used for Group ICA were always included in the training set, avoiding overlap with validation or test sets. This step minimized bias and maintained the reliability of our results. Experimental outcomes are summarized in Tables 5 and 6, presenting the average test performance and standard deviations of the fine-tuned models.

**Discussion** This study demonstrates that integrating Group ICA-based dimensionality reduction with the SwiFT Transformer architecture significantly enhances the prediction of neurodevelopmental outcomes from neonatal fMRI data. By extracting biologically meaningful features through ICA and employing multi-label learning, our approach balances dimensionality reduction with the preservation of critical neural information. The SwiFT Transformer uniquely learns complex spatiotemporal patterns in early brain development directly from 4D fMRI data, leveraging its attention-based architecture to model both local and global dependencies. These findings highlight the potential of combining neuroscience-driven feature engineering with advanced machine learning to improve both interpretability and predictive accuracy, providing a robust framework for neurodevelopmental research and clinical applications.

Our results indicate that the choice of ICA dimensionality (25 vs. 100 components) does not significantly affect the model’s predictive performance in regression or classification tasks. This invariance suggests that ICA robustly captures the essential features of neural activity, regardless of the specific number of components used. Both configurations effectively isolate key brain networks while filtering out noise, ensuring that critical information relevant to neurodevelopmental outcomes is retained. This finding reinforces the adaptability of ICA-based dimensionality reduction as a reliable preprocessing step for fMRI analysis.

As shown in Table 5, single-label learning with ICA-extracted features slightly outperforms predictions using raw fMRI data, particularly for language skill classification and motor skill regression. These results demonstrate that dimensionality reduction through ICA retains critical neural information while effectively filtering out noise. By isolating independent components that likely represent functional networks related to cognitive, language, and motor development, ICA enables the model to better capture the neural

patterns underlying developmental outcomes. This process not only preserves essential details but also reduces the computational complexity associated with high-dimensional raw data.

Furthermore, ICA’s ability to extract biologically meaningful components allows the model to focus on critical brain networks, improving accuracy and robustness over using the more variable and noisy raw data. This targeted approach highlights the value of combining neuroscience-driven feature engineering with advanced machine learning methods. When paired with multi-label learning, as shown in Table 6, ICA-extracted features yield the best results, demonstrating similar performance boosts to those observed with raw fMRI volumes. This underscores the effectiveness of integrating ICA into our pipeline to enhance predictive power and model efficiency.

Table 5: Mean performance with standard deviation through 5-cross-validation by using IC-extracted features, facilitating single-label predictions.

ICs	Cog		
	$MSE_{adj}$	MAE	$MAE_{adj}$
25	127.2 $\pm$ 6.9	<b>0.74<math>\pm</math>0.03</b>	<b>8.7<math>\pm</math>0.4</b>
100	<b>126.8<math>\pm</math>8.2</b>	0.74 $\pm$ 0.07	8.7 $\pm$ 0.9
	ACC	$ACC_{bal}$	AUC
25	93.7 $\pm$ 1.5	<b>55.7<math>\pm</math>4.0</b>	<b>56.6<math>\pm</math>4.7</b>
100	<b>93.8<math>\pm</math>1.3</b>	52.4 $\pm$ 1.2	53.1 $\pm$ 2.4
ICs	Lang		
	$MSE_{adj}$	MAE	$MAE_{adj}$
25	<b>293.4<math>\pm</math>11.4</b>	0.82 $\pm$ 0.02	12.6 $\pm$ 0.3
100	299.5 $\pm$ 13.3	<b>0.8<math>\pm</math>0.02</b>	<b>12.4<math>\pm</math>0.3</b>
	ACC	$ACC_{bal}$	AUC
25	<b>84.0<math>\pm</math>2.9</b>	<b>57.8<math>\pm</math>2.3</b>	<b>58.3<math>\pm</math>2.8</b>
100	82.5 $\pm$ 3.5	56.3 $\pm$ 1.8	57.2 $\pm$ 2.4
ICs	Mot		
	$MSE_{adj}$	MAE	$MAE_{adj}$
25	95.7 $\pm$ 9.2	0.76 $\pm$ 0.04	7.7 $\pm$ 0.3
100	<b>94.0<math>\pm</math>10.3</b>	<b>0.75<math>\pm</math>0.03</b>	<b>7.5<math>\pm</math>0.2</b>
	ACC	$ACC_{bal}$	AUC
25	<b>95.2<math>\pm</math>0.7</b>	55.3 $\pm$ 3.6	56.1 $\pm$ 3.8
100	92.8 $\pm$ 0.9	<b>55.6<math>\pm</math>3.1</b>	<b>56.7<math>\pm</math>3.4</b>

### 3.5 Comparative Analysis

We have summarized our experimental results via boxplots in Figure 4, while omitting results obtained via transfer-learning and higher-dimensional ICs due to no statistically significant performance changes. Across all metrics, Multi-ICA demonstrates significant and consistent improvements over the best-performing baseline model for most tasks, particularly in Cognitive MAE ( $p = 0.004$ ) and Motor MAE ( $p = 0.002$ ). These results underscore the advantage of incorporating ICA-extracted features in the regression of cognitive

Table 6: Mean performance with standard deviation through 5-cross-validation by using IC-extracted features, facilitating multi-label predictions.

ICs	Cog		
	$MSE_{adj}$	MAE	$MAE_{adj}$
25	<b>119.8<math>\pm</math>10.9</b>	<b>0.61<math>\pm</math>0.06</b>	<b>8.1<math>\pm</math>0.55</b>
100	121.1 $\pm$ 7.0	0.65 $\pm$ 0.07	8.6 $\pm$ 0.8
	ACC	$ACC_{bal}$	AUC
25	95.0 $\pm$ 1.4	<b>60.6<math>\pm</math>1.6</b>	<b>62.2<math>\pm</math>1.6</b>
100	<b>95.8<math>\pm</math>1.3</b>	59.4 $\pm$ 1.8	61.6 $\pm$ 1.4
ICs	Lang		
	$MSE_{adj}$	MAE	$MAE_{adj}$
25	<b>212.1<math>\pm</math>17.2</b>	<b>0.85<math>\pm</math>0.02</b>	<b>11.4<math>\pm</math>0.4</b>
100	221.1 $\pm$ 20.4	0.86 $\pm$ 0.03	11.5 $\pm$ 0.5
	ACC	$ACC_{bal}$	AUC
25	<b>83.9<math>\pm</math>2.6</b>	62.2 $\pm$ 0.9	62.9 $\pm$ 1.2
100	81.3 $\pm$ 3.3	<b>62.7<math>\pm</math>1.3</b>	<b>63.8<math>\pm</math>1.7</b>
ICs	Mot		
	$MSE_{adj}$	MAE	$MAE_{adj}$
25	<b>90.1<math>\pm</math>9.6</b>	<b>0.53<math>\pm</math>0.04</b>	<b>7.0<math>\pm</math>0.5</b>
100	90.3 $\pm$ 10.5	0.55 $\pm$ 0.04	7.1 $\pm$ 0.6
	ACC	$ACC_{bal}$	AUC
25	94.5 $\pm$ 1.3	<b>58.4<math>\pm</math>1.5</b>	<b>60.1<math>\pm</math>1.7</b>
100	<b>95.0<math>\pm</math>1.5</b>	57.2 $\pm$ 2.1	59.7 $\pm$ 1.5

and motor delays.

Similarly, for regression tasks, significant reductions in cognitive regression  $MSE_{adj}$  ( $p = 0.036$ ) and language regression  $MSE_{adj}$  ( $p = 0.008$ ) highlight the robustness of the Multi-ICA approach in modeling complex developmental outcomes. Importantly, these improvements hold across multiple target domains, reinforcing the utility of a multi-label learning paradigm.

In classification, Multi-ICA also achieves significant improvements in language classification accuracy ( $p = 0.004$ ) and motor classification AUC ( $p = 0.044$ ), while maintaining competitive performance across most other metrics. However, some metrics – such as cognitive classification AUC ( $p = 0.413$ ) – did not show statistically significant differences compared to the baseline. These results suggest that the model’s performance in certain domains, particularly language-related tasks, may benefit from further domain-specific optimization.

Overall, Multi-ICA paired with multi-label learning consistently outperforms the strongest baseline model, confirming its utility for both regression and classification tasks in the context of predicting developmental outcomes.

## 4 Interpretation via Integrated Gradients

As in the original SwiFT study (Kim et al. 2023), we used Integrated Gradient with Smoothgrad sQuare (IG-SQ), implemented through the Captum framework (Rahman et al.



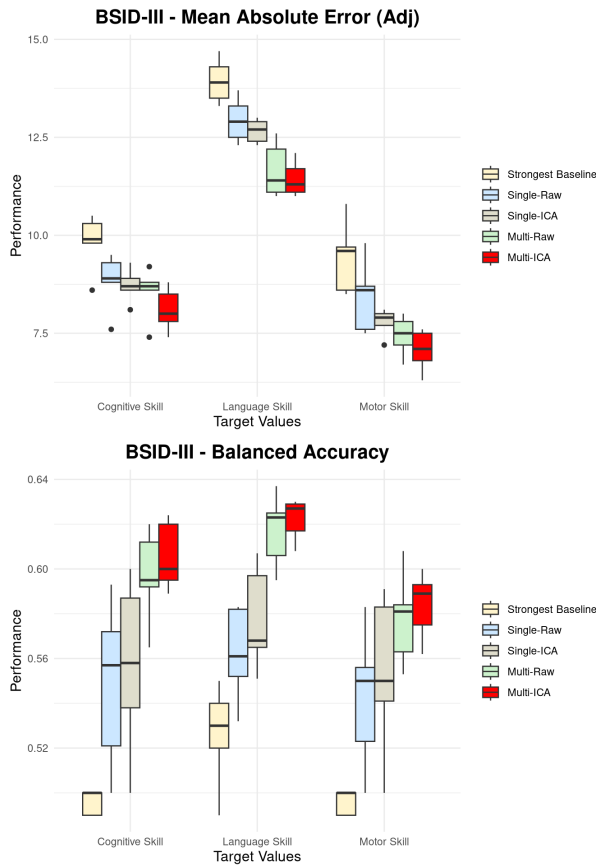


Figure 4: Overview of the models' predictive power via 5-fold cross-validation for BSID-III regression ( $MAE_{adj}$ ) and classification ( $ACC_{bal}$ ). The strongest baseline was taken to represent baseline performance. Performance by transfer-learning and 100 ICs was omitted due to no statistically significant performance changes.

2022) (Adebayo et al. 2018) (Kokhlikyan et al. 2020). This method allowed us to identify spatial representations in brain regions that contribute to Bayley-III classification tasks. This analysis was based on the best-performing model, which combined multi-label prediction with ICA-extracted features. The use of independent components (ICs) facilitated neuroscientifically more useful interpretations by linking model outputs to known functional networks (Beckmann et al. 2009).

For each test sample, we generated 4D IG-SQ maps and excluded misclassified instances to ensure the validity of interpretations. The resulting attribution maps were normalized, Gaussian-smoothed, and averaged across subjects to identify spatial patterns consistently associated with cognitive, language, and motor outcomes. Additionally, we aggregated these maps across ICs to derive comprehensive interpretations of brain activity relevant to each developmental domain.

The analysis revealed distinct brain regions whose spatiotemporal dynamics contribute to each developmental out-

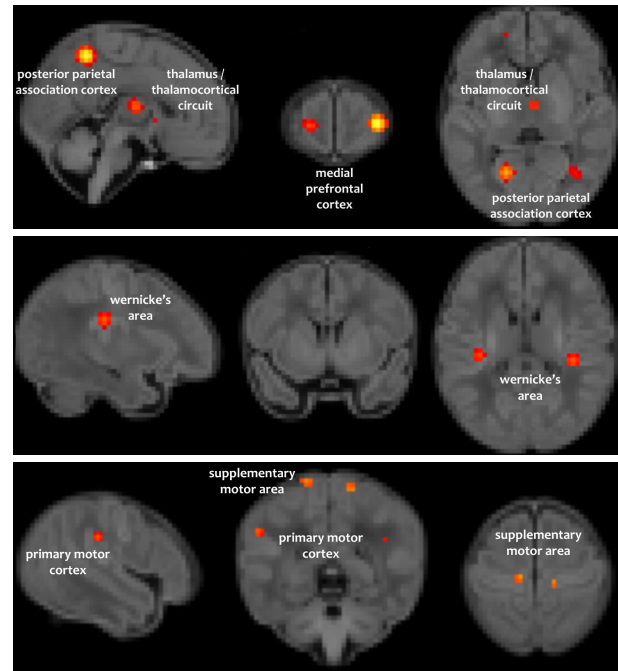


Figure 5: Interpretation maps with thresholded Integrated Gradients (IG) maps averaged across ICs for risk of cognitive (top), language (middle) and motor (bottom) delay.

come (Figure 5). This data-driven approach reveals meaningful neuroscientific interpretations, demonstrating that regions within the distinct functional networks correspond closely to neurodevelopmental outcomes, reflecting their established roles in cognitive and neural development. For cognitive delay risk, activations were observed in the medial prefrontal cortex (coronal view), thalamocortical circuit (sagittal and axial view), and posterior parietal association cortex (sagittal view). These findings align with neuroscience literature: the identified brain regions are key to early sensory processing, attention, executive function, and spatial cognition, all foundational to normal cognitive development (Mair et al. 2022) (Benarroch and Benarroch 2021) (Shomstein 2012).

In Figure 6, network-level predictions are further explored ICA-extracted features. For instance, IC5 likely represents the Executive Control Network (ECN) (Li et al. 2019), a critical network for cognitive functions such as attention and decision-making. Its contribution to the overall interpretation, as shown in Figure 5, is evident through activations in the medial prefrontal cortex, a hallmark region of the ECN.

For linguistic delay risk (middle), activations in Wernicke's area align with its well-documented role in language comprehension and development (Binder 2015). Similarly, for motor skill delays (bottom), activations in the primary motor cortex and supplementary motor areas (SMA) highlight their roles in gross and fine motor control and motor pattern learning, respectively (Graziano 2006; Tanji and Shima 1994).

These findings reinforce the model's ability to capture

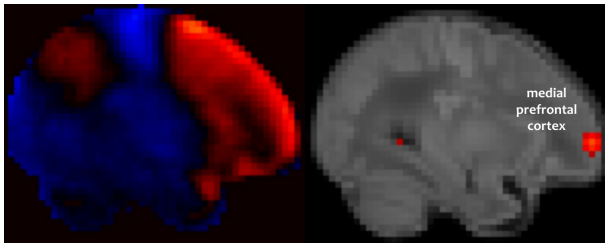


Figure 6: A glimpse into network-level interpretations, focusing on IC 5 (left), possibly representing the Executive Control Network (ECN). For predicting the risk of cognitive delay, can see how this brain-network adds to activation in the medial prefrontal cortex (right).

neurobiologically meaningful spatiotemporal patterns, as discussed earlier. By integrating both spatial localization and temporal dynamics of brain activity, the model effectively associates developmental delays with functional neural circuits. This alignment with established neuroscience underscores the robustness of our approach, demonstrating how machine learning can provide interpretable insights into the neural basis of developmental outcomes.

## 5 Concluding Remarks

In this study, we demonstrated that the SwiFT (Swin 4D fMRI Transformer) model provides a significant improvement in evaluating neonatal fMRI data for predicting neurodevelopmental outcomes. By integrating multi-label learning and leveraging ICA-extracted features, we achieved enhanced predictive accuracy while improving model interpretability. These advances suggest that SwiFT has the potential to play a pivotal role in the early detection of developmental delays, paving the way for personalized therapeutic interventions for at-risk neonates.

Despite these accomplishments, limitations remain. The imbalanced nature of the dataset poses a challenge, impacting the reliability of the classification tasks. While our approach partially mitigated this issue, future work should explore advanced strategies for handling data imbalance (Buda, Maki, and Mazurowski 2018). Additionally, further validation of ICA-extracted features as proxies for brain-network-level mechanisms is necessary to strengthen the biological interpretability of our findings. Also, expanding this framework to include datasets from other age groups, such as toddlers, children, and adults, could enhance the generalizability of the model. Finally, extending the multi-label learning paradigm to incorporate additional target variables, such as the Q-CHAT score for early autism screening, offers an exciting direction for future research.

In conclusion, this work establishes a robust foundation for advancing predictive and interpretable models of neurodevelopment. With continued refinement and access to diverse, large-scale datasets, the SwiFT Transformer holds significant potential for innovations in neuroscience and personalized medicine.

## References

- Adebayo, J.; Gilmer, J.; Goodfellow, I.; and Kim, B. 2018. Local Explanation Methods for Deep Neural Networks Lack Sensitivity to Parameter Values. *arXiv:1810.03307*.
- Alfaro-Almagro, F.; Jenkinson, M.; Bangerter, N. K.; Andersson, J. L.; Griffanti, L.; Douaud, G.; Sotiropoulos, S. N.; Jbabdi, S.; Hernandez-Fernandez, M.; Vallee, E.; Vidaurre, D.; Webster, M.; McCarthy, P.; Rorden, C.; Daducci, A.; Alexander, D. C.; Zhang, H.; Dragonu, I.; Matthews, P. M.; Miller, K. L.; and Smith, S. M. 2018a. Image processing and Quality Control for the first 10,000 brain imaging datasets from UK Biobank. *NeuroImage*, 166: 400–424.
- Alfaro-Almagro, F.; Jenkinson, M.; Bangerter, N. K.; Andersson, J. L.; Griffanti, L.; Douaud, G.; Sotiropoulos, S. N.; Jbabdi, S.; Hernandez-Fernandez, M.; Vallee, E.; et al. 2018b. Image processing and quality control for the first 10,000 brain imaging datasets from UK Biobank. *Neuroimage*, 166: 400–424.
- Beckmann, C.; Mackay, C.; Filippini, N.; and Smith, S. 2009. Group comparison of resting-state fMRI data using multi-subject ICA and dual regression. *NeuroImage*, 47: S148. Organization for Human Brain Mapping 2009 Annual Meeting.
- Beckmann, C. F.; and Smith, S. M. 2004. Probabilistic Independent Component Analysis for Functional Magnetic Resonance Imaging. *IEEE Transactions on Medical Imaging*, 23(2): 137–152.
- Benarroch, E. E.; and Benarroch, E. E. 2021. 477Thalamus and Thalamocortical Interactions. In *Neuroscience for Clinicians: Basic Processes, Circuits, Disease Mechanisms, and Therapeutic Implications*. Oxford University Press. ISBN 9780190948894.
- Binder, J. R. 2015. The Wernicke area: Modern evidence and reinterpretation. *Neurology*, 85(1): 15–21.
- Buda, M.; Maki, A.; and Mazurowski, M. A. 2018. A systematic study of the class imbalance problem in convolutional neural networks. *Neural Networks*, 106: 249–259.
- Casey, B. J.; Cannonier, T.; Conley, M. I.; Cohen, A. O.; Barch, D. M.; Heitzeg, M. M.; Soules, M. E.; Teslovich, T.; Dellarco, D. V.; Garavan, H.; et al. 2018. The adolescent brain cognitive development (ABCD) study: imaging acquisition across 21 sites. *Developmental Cognitive Neuroscience*, 32: 43–54.
- Chen, T.; and Guestrin, C. 2016. XGBoost: A Scalable Tree Boosting System. In *Proceedings of the 22nd ACM SIGKDD International Conference on Knowledge Discovery and Data Mining*, KDD '16, 785–794. New York, NY, USA: Association for Computing Machinery. ISBN 9781450342322.
- Dave, I.; Gupta, R.; Rizve, M. N.; and Shah, M. 2022. TCLR: Temporal contrastive learning for video representation. *Computer Vision and Image Understanding*, 219: 103406.
- Eyre, M.; Fitzgibbon, S. P.; Ciarrusta, J.; Cordero-Grande, L.; Price, A. N.; Poppe, T.; Schuh, A.; Hughes, E.; O’Keeffe, C.; Brandon, J.; Cromb, D.; Vecchiato, K.; Andersson, J.;



- Duff, E. P.; Counsell, S. J.; Smith, S. M.; Rueckert, D.; Hajnal, J. V.; Arichi, T.; O’Muircheartaigh, J.; Batalle, D.; and Edwards, A. D. 2021. The Developing Human Connectome Project: typical and disrupted perinatal functional connectivity. *Brain*, 144(7): 2199–2213.
- Fitzgibbon, S. P.; Harrison, S. J.; Jenkinson, M.; Baxter, L.; Robinson, E. C.; Bastiani, M.; Bozek, J.; Karolis, V.; Cordero Grande, L.; Price, A. N.; Hughes, E.; Makropoulos, A.; Passerat-Palmbach, J.; Schuh, A.; Gao, J.; Farahibozorg, S.-R.; O’Muircheartaigh, J.; Ciarrusta, J.; O’Keeffe, C.; Brandon, J.; Arichi, T.; Rueckert, D.; Hajnal, J. V.; Edwards, A. D.; Smith, S. M.; Duff, E.; and Andersson, J. 2020. The developing Human Connectome Project (dHCP) automated resting-state functional processing framework for newborn infants. *NeuroImage*, 223: 117303.
- Gal, S.; Tik, N.; Bernstein-Eliav, M.; and Tavor, I. 2022. Predicting individual traits from unperformed tasks. *NeuroImage*, 249: 118920.
- Gondová, A.; Neumane, S.; Leprince, Y.; Mangin, J.-F.; Arichi, T.; and Dubois, J. 2023. Predicting neurodevelopmental outcomes from neonatal cortical microstructure: A conceptual replication study. *Neuroimage: Reports*, 3(2): 100170.
- Graziano, M. S. A. 2006. The organization of behavioral repertoire in motor cortex. *Annual Review of Neuroscience*, 29: 105–134.
- He, L.; Li, H.; Holland, S. K.; Yuan, W.; Altabe, M.; and Parikh, N. A. 2018. Early prediction of cognitive deficits in very preterm infants using functional connectome data in an artificial neural network framework. *NeuroImage: Clinical*, 18: 290–297.
- He, L.; Li, H.; Wang, J.; Chen, M.; Gozdas, E.; Dillman, J. R.; and Parikh, N. A. 2020a. A multi-task, multi-stage deep transfer learning model for early prediction of neurodevelopment in very preterm infants. *Scientific Reports*, 10(1): 15072.
- He, L.; Li, H.; Wang, J.; Chen, M.; Gozdas, E.; Dillman, J. R.; and Parikh, N. A. 2020b. A multi-task, multi-stage deep transfer learning model for early prediction of neurodevelopment in very preterm infants. *Scientific Reports*, 10(1): 15072.
- Hyvärinen, A. 1999. Fast and Robust Fixed-Point Algorithms for Independent Component Analysis. *IEEE Transactions on Neural Networks*, 10(3): 626–634.
- Johnson, S.; Moore, T.; and Marlow, N. 2014. Using the Bayley-III to assess neurodevelopmental delay: which cut-off should be used? *Pediatric Research*, 75(5): 670–674.
- Kan, X.; Dai, W.; Cui, H.; Zhang, Z.; Guo, Y.; and Yang, C. 2022. Brain Network Transformer. arXiv:2210.06681.
- Kawahara, J.; Brown, C. J.; Miller, S. P.; Booth, B. G.; Chau, V.; Grunau, R. E.; Zwicker, J. G.; and Hamarneh, G. 2017. BrainNetCNN: Convolutional neural networks for brain networks; towards predicting neurodevelopment. *NeuroImage*, 146: 1038–1049.
- Kim, P. Y.; Kwon, J.; Joo, S.; Bae, S.; Lee, D.; Jung, Y.; Yoo, S.; Cha, J.; and Moon, T. 2023. SwiFT: Swin 4D fMRI Transformer. arXiv:2307.05916.
- Kokhlikyan, N.; Miglani, V.; Martin, M.; Wang, E.; Alsallakh, B.; Reynolds, J.; Melnikov, A.; Kliushkina, N.; Araya, C.; Yan, S.; and Reblitz-Richardson, O. 2020. Captum: A unified and generic model interpretability library for PyTorch. *CoRR*, abs/2009.07896.
- Li, C.; Deng, Y.; He, Y.; Zhai, H.; and Jia, F. 2019. The development of brain functional connectivity networks revealed by resting-state functional magnetic resonance imaging. *Neural Regeneration Research*, 14(8): 1419–1429.
- Li, Q.; Xia, M.; Zeng, D.; Xu, Y.; Sun, L.; Liang, X.; Xu, Z.; Zhao, T.; Liao, X.; Yuan, H.; Liu, Y.; Huo, R.; Li, S.; and He, Y. 2024. Development of segregation and integration of functional connectomes during the first 1,000 days. *Cell Reports*, 43(5): 114168.
- Lin, T.-Y.; Goyal, P.; Girshick, R.; He, K.; and Dollár, P. 2018. Focal Loss for Dense Object Detection. arXiv:1708.02002.
- Mair, R. G.; Francoeur, M. J.; Krell, E. M.; and Gibson, B. M. 2022. Where Actions Meet Outcomes: Medial Prefrontal Cortex, Central Thalamus, and the Basal Ganglia. *Frontiers in Behavioral Neuroscience*, 16.
- Miller, K. L.; Alfaro-Almagro, F.; Bangerter, N. K.; Thomas, D. L.; Yacoub, E.; Xu, J.; Bartsch, A. J.; Jbabdi, S.; Sotiropoulos, S. N.; Andersson, J. L.; et al. 2016a. Multimodal population brain imaging in the UK Biobank prospective epidemiological study. *Nature Neuroscience*, 19(11): 1523–1536.
- Miller, K. L.; Alfaro-Almagro, F.; Bangerter, N. K.; Thomas, D. L.; Yacoub, E.; Xu, J.; Bartsch, A. J.; Jbabdi, S.; Sotiropoulos, S. N.; Andersson, J. L. R.; Griffanti, L.; Douaud, G.; Okell, T. W.; Weale, P.; Dragonu, I.; Garratt, S.; Hudson, S.; Collins, R.; Jenkinson, M.; Matthews, P. M.; and Smith, S. M. 2016b. Multimodal Population Brain Imaging in the UK Biobank Prospective Epidemiological Study. *Nature Neuroscience*, 19(11): 1523–1536.
- Rahman, M. M.; Mahmood, U.; Lewis, N.; Gazula, H.; Fedorov, A.; Fu, Z.; Calhoun, V. D.; and Plis, S. M. 2022. Interpreting models interpreting brain dynamics. *Scientific Reports*, 12(1): 12023.
- Schuh, A.; Makropoulos, A.; Robinson, E. C.; Cordero Grande, L.; Hughes, E.; Hutter, J.; Price, A. N.; Murgasova, M.; Teixeira, R. P. A. G.; Tusor, N.; Steinweg, J. K.; Victor, S.; Rutherford, M. A.; Hajnal, J. V.; Edwards, A. D.; and Rueckert, D. 2018. Unbiased construction of a temporally consistent morphological atlas of neonatal brain development. *bioRxiv*.
- Shomstein, S. 2012. Cognitive functions of the posterior parietal cortex: top-down and bottom-up attentional control. *Frontiers in Integrative Neuroscience*, 6.
- Smith, S. M.; Beckmann, C. F.; Andersson, J.; Auerbach, E. J.; Bijsterbosch, J.; Douaud, G.; Duff, E.; Feinberg, D. A.; Griffanti, L.; Harms, M. P.; Kelly, M.; Laumann, T.; Miller, K. L.; Moeller, S.; Petersen, S.; Power, J.; Salimi-Khorshidi, G.; Snyder, A. Z.; Vu, A. T.; Woolrich, M. W.; Xu, J.; Yacoub, E.; Ugurbil, K.; Van Essen, D. C.; and Glasser, M. F. 2013. Resting-state fMRI in the Human Connectome

Project. *NeuroImage*, 80: 144–168. Mapping the Connectome.

Smith, S. M.; Fox, P. T.; Miller, K. L.; Glahn, D. C.; Fox, P. M.; Mackay, C. E.; Filippini, N.; Watkins, K. E.; Toro, R.; Laird, A. R.; and Beckmann, C. F. 2009. Correspondence of the brain's functional architecture during activation and rest. *Proceedings of the National Academy of Sciences*, 106(31): 13040–13045.

Smith, S. M.; Hyvärinen, A.; Varoquaux, G.; Miller, K. L.; and Beckmann, C. F. 2014. Group-PCA for Very Large fMRI Datasets. *NeuroImage*, 101: 738–749.

Tange, O. 2023. GNU Parallel 20240622 ('34 counts'). GNU Parallel is a general parallelizer to run multiple serial command line programs in parallel without changing them.

Tanji, J.; and Shima, K. 1994. Role of supplementary motor area cells in planning and executing sequential movements. *Brain Research*, 619(1-2): 260–263.

Tustison, N. J.; Cook, P. A.; Holbrook, A. J.; Johnson, H. J.; Muschelli, J.; Devenyi, G. A.; Duda, J. T.; Das, S. R.; Cullen, N. C.; Gillen, D. L.; Yassa, M. A.; Stone, J. R.; Gee, J. C.; and Avants, B. B. 2021. The ANTsX ecosystem for quantitative biological and medical imaging. *Scientific Reports*, 11(1): 9068.

Van Essen, D. C.; Smith, S. M.; Barch, D. M.; Behrens, T. E.; Yacoub, E.; Ugurbil, K.; and Consortium, W.-M. H. 2013. The Wu-Minn Human Connectome Project: an overview. *Neuroimage*, 80: 62–79.

Xia, Y.; Zhao, J.; Xu, Y.; Duan, D.; Xia, M.; Jeon, T.; Ouyang, M.; Chalak, L.; Rollins, N.; Huang, H.; and He, Y. 2024. Development of sensorimotor-visual connectome gradient at birth predicts neurocognitive outcomes at 2 years of age. *iScience*, 27(2): 108981.